Ionized Phenol and Its Isomers in the Gas Phase

Hung Thanh Le,[†,‡] Robert Flammang,[§] Pascal Gerbaux,[§] Guy Bouchoux,[||] and Minh Tho Nguyen*[,†]

Department of Chemistry, University of Leuven, Celestijnenlaan 200F, B-3001 Leuven, Belgium, Laboratoire de Chimie Organique, Université de Mons-Hainaut, Avenue Maistriau 19, B-7000 Mons, Belgium, Laboratoire des Mécanismes Réactionnels, UMR CNRS 7651, Ecole Polytechnique, F-91128 Palaiseau cedex, France, and Group of Computational Chemistry, Faculty of Chemical Engineering, HoChiMinh City University of Technology, Vietnam

Received: July 12, 2001; In Final Form: October 15, 2001

Protonated 4-bromophenol and 4-bromoanisole produced by methane chemical ionization are found to easily be dehalogenated upon high (8 keV) or low (20−30 eV) energy collisional activation giving essentially phenol and anisole radical cations, respectively. Under similar conditions, protonated unsubstituted anisole is also readily demethylated generating the phenol ion but not cyclohexadienone ions. Other nonconventional isomers of ionized phenol are only detected by MS/MS/MS experiments performed on $[M-CO]^{\bullet+}$ ions from salicylaldehyde. (U)B3LYP/6-311++G(d,p) and CASPT2/6-31G(d,p) calculations indicate the higher stability of the phenol radical cation with respect to the other six-membered-ring isomers. The least energy demanding fragmentation, namely, the decarbonylation, is shown to involve the intermediacy of six-membered ketones, open-chain ketenes, and five-membered cyclopentadiene isomeric ions. The rate determining step corresponds to the enol−keto interconversion with an energy barrier of about 276 kJ/mol relative to the phenol ion, which is markedly smaller than that required for hydrogen atom loss, deprotonation, or CO loss from an open-chain form. This suggests a crucial role played by the solvent in the readiness of the deprotonation of phenol ions in nonpolar media. The adiabatic ionization energy of phenol is evaluated as $IE_a(C_6H_5O) = 8.35 \pm 0.2$ eV (exptl: 8.49 eV), and the proton affinity of the phenoxy radical is evaluated as $PA(C_6H_5O) = 863 \pm 10$ kJ/mol (exptl: 860 kJ/mol), PA(phenol) = 826 ± 10 kJ/mol (exptl: 818 kJ/mol), and PA(anisole) = 848 ± 10 kJ/mol.

1. Introduction

The chemistry of phenols in which a hydroxyl group (−OH) is attached to a benzenic ring has generated continuing interest in the last century.[1] Compounds bearing this functional group have several applications indispensable in our daily life. For example, they constitute, among others, an important class of antioxidants that inhibit the oxidative degradation of organic materials including a large number of biological aerobic organisms and commercial products.[2] In human blood plasma, α-tocopherol, well-known as vitamin E, is proved to be the most efficient phenol derivative to date to trap the damaging peroxy radicals (ROO).[3] In fact, phenols owe their activity to their ability to scavenge radicals by hydrogen or electron transfer in much faster processes than radical attacks on an organic substrate. Following the transfer of the phenolic hydrogen atom, phenols are normally converted into phenoxy radicals.[4−6]

Because of their relatively low ionization energies (ca. 8.4 eV), phenols are also good electron donor solutes. Recent experimental studies of phenols in nonprotic solvents[7−10] showed that ionized solvent molecules react with phenol to yield not only phenol radical cations by electron transfer but also phenoxy radicals by hydrogen transfer. An obvious question is whether under these conditions the latter radicals are formed from ionized phenols rather than by direct hydrogen abstraction, because proton-transfer reactions could be facilitated upon ionization. This also raises a question about the influence of solvent properties on the mechanism and kinetics of the deprotonation processes.[11−12]

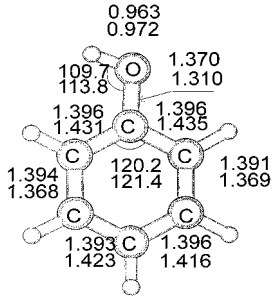

Figure 1. Selected (U)B3LYP/6-311++G(d) bond distances and angles of the neutral ($^1A'$, upper values) and ionized ($^2A''$, lower values) phenol.

SCHEME 1

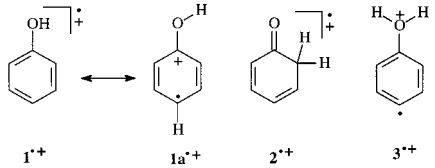

* To whom correspondence should be addressed. Fax: 32-16-32 79 92. E-mail: minh.nguyen@chem.kuleuven.ac.be.
† University of Leuven.
‡ HoChiMinh City University of Technology.
§ Université de Mons-Hainaut.
|| Ecole Polytechnique.

10.1021/jp012679e CCC: $20.00
Published on Web 12/01/2001

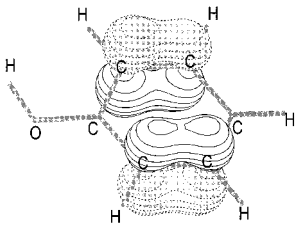

HOMO-1 orbital

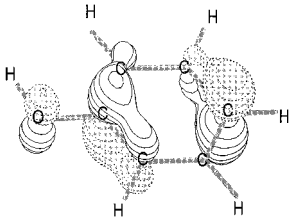

HOMO orbital

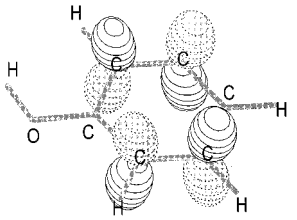

LUMO orbital

Figure 2. Shape of the frontier orbitals of neutral phenol computed using HF/6-31G(d,p) wave functions.

One way of addressing the above questions is to approach the stability of the phenol ion system in the gas phase. By definition, gas-phase properties have an intrinsic character and could be modified by the environment. Although ionized phenol $\mathbf{1}^{\bullet+}$ (cf. Scheme 1) and its cyclohexa-2,4-dienone isomer $\mathbf{2}^{\bullet+}$ have been studied in numerous earlier ionization and mass spectrometric studies,[13−21] thermochemical parameters of these isomers are rather scarce.[22−26] As far as we are aware, information on other nonconventional isomers such as the distonic ion $\mathbf{3}^{\bullet+}$ is non existent (Scheme 1). In addition, the mechanism of the CO loss upon ionization of phenol is not fully understood. Recent studies on aromatic systems such as benzonitrile,[27] benzaldehyde,[28] or aniline[29] have showed that the classical ions and their distonic isomers generated by simple 1,2-H shifts within the ring are detectable gas-phase species. In view of the lack of quantitative information on the phenol ion isomers, we set out to construct a lower-lying portion of the $[C_6H_6O]^{\bullet+}$ potential energy surface using ab initio quantum chemical methods in order to unravel their gaseous phase unimolecular reactivity. The intrinsic gas-phase properties could provide, in addition, some insights into their behavior in solvents. The study is further pursued by an experimental investigation using the most recent tandem mass spectrometric techniques (MS^3) in an attempt to generate some nonclassical ion isomers. The computational results will be presented first, whereas the MS results will be discussed in a subsequent section.

2. Quantum Chemical Calculations

All calculations are performed with the Gaussian 98 set of programs.[30] Geometrical parameters of the structures considered are initially optimized and subsequently characterized by harmonic vibrational analyses using the density functional theory with the popular hybrid B3LYP functionals,[31] in conjunction with the dp-polarized 6-31G(d,p) basis set and the unrestricted formalism (UB3LYP) for open-shell systems. The zero-point energy corrections (ZPE) to relative energies are also obtained at this level.

Geometries of the relevant stationary points are then reoptimized making use of the larger 6-311++G(d,p) basis set including diffuse functions. Recent theoretical studies[32−35] on similar systems demonstrated that the B3LYP method provides the relative energies comparable to those derived using the molecular orbital coupled-cluster theory. The absolute deviations between B3LYP and CCSD(T) values, when using the same basis set, amount to an average of about 10 kJ/mol. In addition, use of the the DFT method allows us to avoid the problem of spin contamination in UHF-reference wave functions by higher spin configurations which is usually severe in many unconventional open-shell species, such as the case of the present study. Spin contamination usually leads to many practical difficulties in the optimization processes and also induces an inherently slow and deceptive convergence of the perturbation and coupled-cluster expansions. To further verify the validity of the B3LYP relative energies, multiconfigurational CASSCF wave functions are also constructed from seven-electron-in-eight-orbital active spaces with the 6-31G(d,p) basis set and B3LYP geometries. The second-order perturbation CASPT2 calculations are equally performed. The CASCF/CASPT2 energies are obtained with the aid of the Molcas program.[36] Throughout this section, bond distances are given in angstrom, bond angles in degrees, and relative energies in kJ/mol. Unless otherwise noted, the latter are derived from (U)B3LYP/6-311++G(d,p) + ZPE calculations.

A. Electronic Structure of the Phenol Radical Cation. The molecular structure, vibrational frequencies, and spin densities of ionized phenol in its ground and excited electronic states have been investigated in earlier detailed theoretical studies using different MO and DFT methods.[13−15,23−25] We supplement here the available information by giving in Figure 1 the selected (U)B3LYP/6-311++G(d,p) geometrical parameters of both neutral and ionized structures. The lowest energy electronic state of phenol radical cation $\mathbf{1}^{\bullet+}$ exhibits a planar geometry and a $^2A''$ symmetry arising from removal of an electron from the π system; therefore, its ground state can be qualified as a $^2\Pi$ state. Following such an ionization, the quasiequal C−C bond (1.40 Å) framework in the neutral phenyl ring becomes the one having alternating longer (1.43 Å) and shorter (1.37 Å) bonds. The latter distance is now closer to that of a typical C═C double bond (1.35 Å). Similarly, the C−O bond is also shortened upon ionization in going from 1.37 (neutral) to 1.31 Å (ionized) but remains however longer than that of a typical C═O double bond (1.22 Å). Such distance changes can be understood from the shape of the HOMO of neutral phenol as displayed in Figure 2. For example, the C−O bond is characterized by an antibonding orbital 2p lobes; therefore, an electron removal is expected to relieve the inherent electron repulsion within that orbital component and thereby to lead to a shortening of the C−O distance. A similar argument could also be applied to the changes of the ring C−C distances. The HOMO-1 as well as the LUMO are mainly phenyl orbitals with the 2p lobes centered on the ortho and meta carbon atoms.

The geometric aspect confers to the phenol ion a certain quinone-like distonic character as seen in $\mathbf{1a}^{\bullet+}$ (cf. Scheme 1) in which the charge and radical centers are located at two different places. This picture is supported by the charge distribution according to the Mulliken population analysis which shows that the para carbon of the ring bears the largest part of

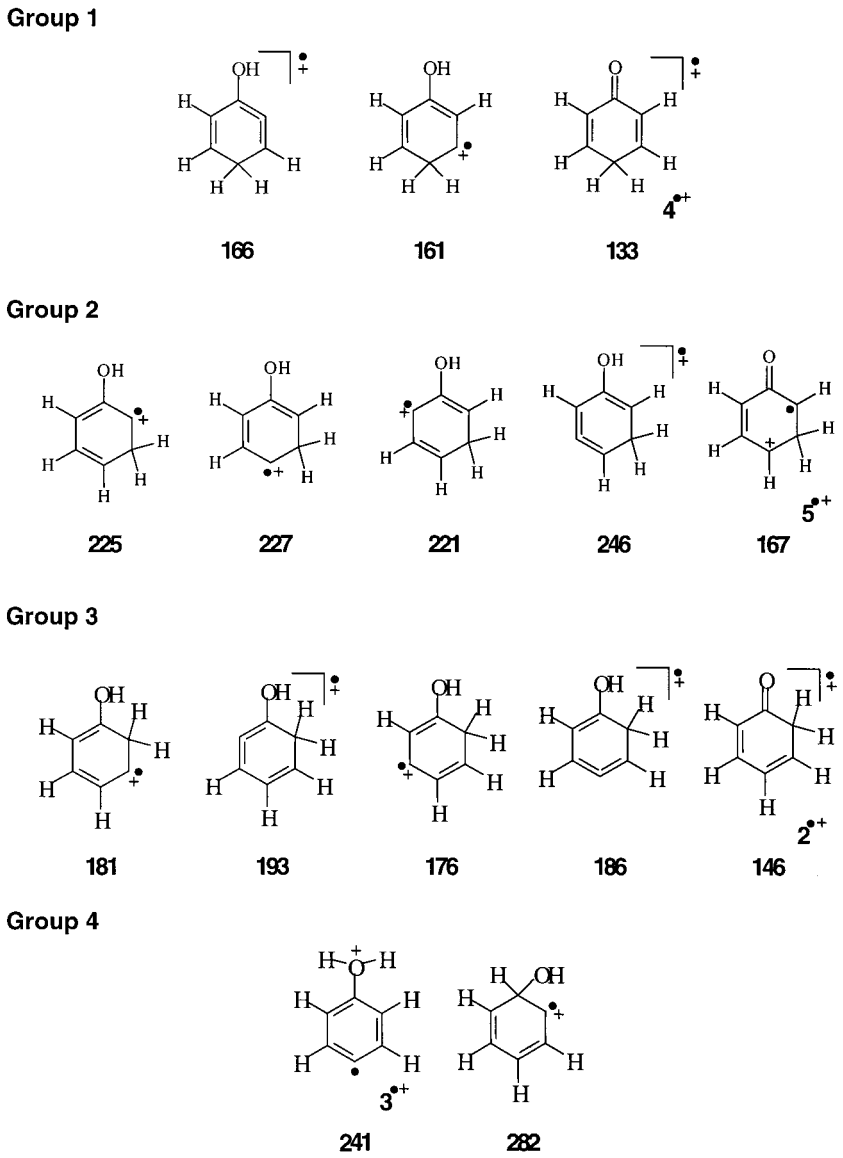

Figure 3. Relative energies of selected isomers of phenol radical cation containing a six-membered ring. Values given in kJ/mol are obtained from UB3LYP/6-311++G(d,p)+ZPE calculations.

the excess electron spin (ca 0.5 e). The positive charge is, as expected, delocalized over the entire ring skeleton.

Attempts to optimize the geometry of the $^2A'$ excited state of the phenol ion are not successful because of a convergence difficulty of the SCF procedure. A single point energy computation of the $^2A'$ state at the $^2A''$- geometry leads to an estimate of 3.30 eV for the vertical $^2A' \leftarrow {}^2A''$ transition. In a recent photoinduced Rydberg ionization spectroscopic study,[14] a B state of the cation at 2.62 eV (21 129 cm^{-1}) was assigned. It is obvious that the DFT methods employed here do not allow us to investigate this interesting problem. We also note that the lowest lying quartet state of phenol ion is a dissociative state giving a triplet phenyl cation plus OH radical that lie about 5.3 eV above the ground state $^2A''$.

Finally, the deprotonation of the phenol ion giving the phenoxy radical $\mathbf{1}^{\bullet+} \rightarrow C_6H_5O$ ($^2A''$) + H^+ is associated with a dissociation energy of 857 (at 0 K) and 863 kJ/mol (298 K). The latter value compares well with the experimental proton affinity of 860 kJ/mol previously determined for the phenoxy radical.[23] Similarly, the PA's (0 K) of phenol and anisole are computed at the same level of theory as PA(phenol) = 820 kJ/mol and PA(anisole) = 842 kJ/mol.

SCHEME 2: B3LYP/6-311++G(d,p)+ZPE Energies of the Oxonium Distonic Isomers and the Transition Structures Connecting Them Relative to Phenol Ion $\mathbf{1}^{\bullet+}$ (kJ/mol)

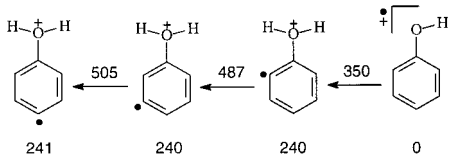

B. Relative Energies of the $(C_6H_6O)^{\bullet+}$ Radical Cations. Figure 3 displays the isomeric structures and their calculated relative energies with respect to the phenol radical cation $\mathbf{1}^{\bullet+}$. There are obviously a large number of possible isomers arising from those of the benzene ring. Here we limit ourselves to the isomers keeping a six-membered ring framework. Starting from $\mathbf{1}^{\bullet+}$, we displace one hydrogen atom from either O or one C atom to another atom, and this exercise results in a creation of the various isomeric groups presented in Figure 3: group 1 includes ions having a CH_2 group at the para (C_4) position, group 2 has it at meta (C_3) position, group 3 has it at the ortho (C_2) position, and group 4 has it at the ipso (C_1) and oxygen positions.

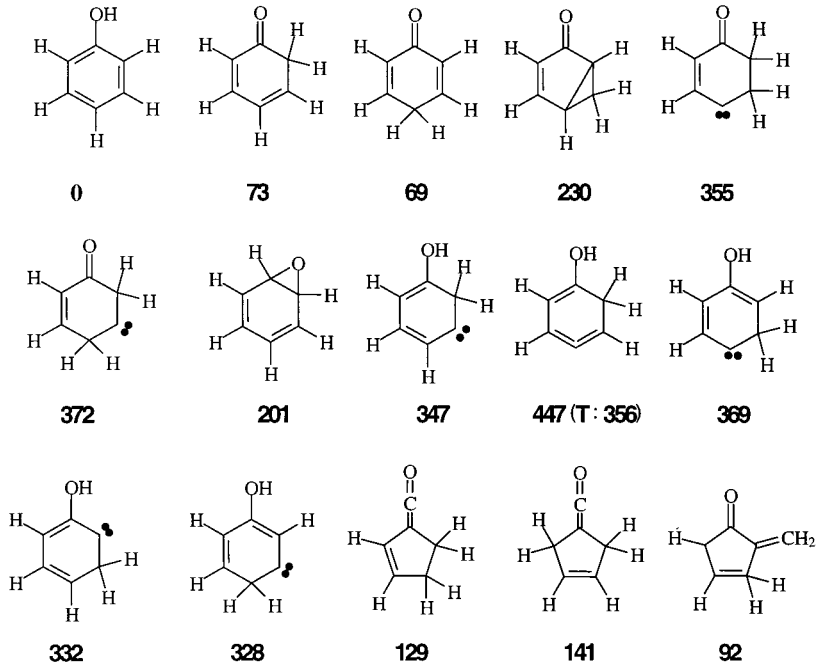

Figure 4. Relative energies of selected isomers of neutral phenol. Values given in kJ/mol are obtained from B3LYP/6-311++G(d,p)+ZPE calculations. The value **T:356** indicates that the corresponding carbene has a triplet ground state which lies 356 kJ/mol above phenol.

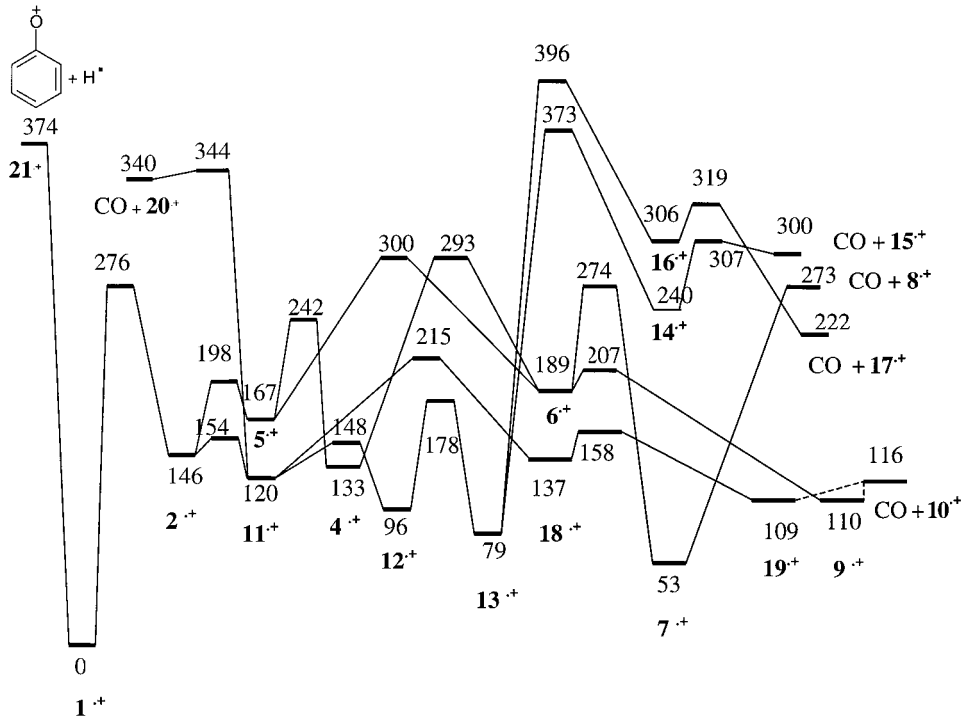

Figure 5. Schematic representation of the $(C_6H_6O)^{\bullet+}$ potential energy surface showing the rearrangements of phenol radical cation leading to a CO loss. Relative energies given in kJ/mol are obtained from B3LYP/6-311++G(d,p) + ZPE calculations.

It turns out that the ionized phenol $\mathbf{1}^{\bullet+}$ represents the most stable form among the six-membered-ring group of isomers. It is worthy to note that keto forms $\mathbf{2}^{\bullet+}$ and $\mathbf{4}^{\bullet+}$ are low-lying isomers which are situated 146 and 133 kJ/mol, respectively, above $\mathbf{1}^{\bullet+}$. This energy ordering within the pair $\mathbf{1}^{\bullet+}$ and $\mathbf{2}^{\bullet+}$ (or $\mathbf{4}^{\bullet+}$) is reminiscent to that encountered for simple keto−enol tautomers.[37] For example, ionized vinyl alcohol is significantly more stable (about 60 kJ/mol) than its keto ion counterpart.[38] The difference in energy observed here between ionized phenol and its keto tautomers is however more pronounced, this point will be clarified below after examination of the neutral counterparts. For its part, the distonic oxonium species $\mathbf{3}^{\bullet+}$ (Scheme 1) belongs to the high energy group of isomers being, relative to $\mathbf{1}^{\bullet+}$, 241 kJ/mol higher in energy. This situation is opposite to the situation met in the ionized aniline system in which the ammonium distonic ion was found to be only 80 kJ/mol above ionized aniline.[39] The other meta and ortho distonic ions have similar energy content and are separated from each other by high energy barriers for 1,2-H shifts (Scheme 2).

To figure out the effect of ionization on the relative stabilities of phenol isomers, we consider a selected set of neutral species whose relative energies are displayed in Figure 4. In the neutral state, only three six-membered-ring structures are in a ∼70 kJ/mol energy range, namely, **1** and both keto forms **2** and **4**. The

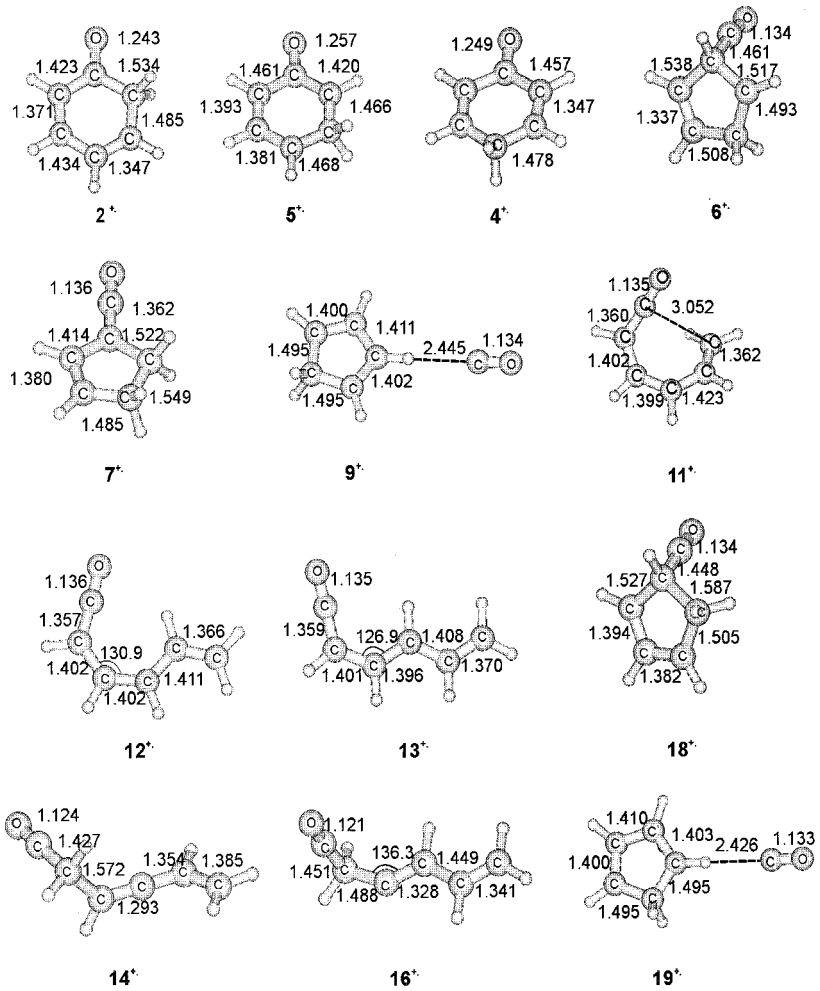

Figure 6. Selected B3LYP/6-311++G(d,p) geometric parameters of the $(C_6H_6O)^{\bullet+}$ equilibrium structures considered. Bond distances are given in angstroms and bond angles in degrees.

carbene, allene, or biradical isomeric forms are strongly destabilized and lie more than 200 kJ/mol above **1**. In contrast, the five-membered ring containing a ketene or a ketone moiety is only 90−140 kJ/mol above phenol. As expected, the phenol **1** is more stable than its tautomers **2** and **4**, and this is partly the origin of the large difference in stability of the corresponding ionized species. In fact, in the phenol series, the aromaticity renders the enol tautomer more stable creating an opposite situation to that observed in the aliphatic series. For example, neutral acetaldehyde is ca. 40 kJ/mol below its enol form, namely, vinyl alcohol. After removal of one electron, the enol structure becomes more stable than the keto form by 60 kJ/mol as recalled above. This stability reversal is due to the large difference in ionization energy between the two structures: 9.14 eV for vinyl alcohol and 10.23 eV for the acetaldehyde in keeping with the fact that it consists of a $\pi_{C=C}$ ionization in the former case and an ionization of an oxygen lone pair in the latter. A comparable situation arises for the phenol (IE = 8.5 eV) and its keto tautomers **2** and **4** (IE ∼10.8 eV). This difference, added to the difference in energy between the neutrals, in favor of the phenol isomer, explains the large energy gaps of $\mathbf{2}^{\bullet+}$ and $\mathbf{4}^{\bullet+}$ with respect to $\mathbf{1}^{\bullet+}$.

C. $(C_6H_6O)^{\bullet+}$ Potential Energy Surface Related to the Rearrangements of the Phenol Radical Cation. In an attempt to identify the most likely transformation routes of the phenol cation, the essential features of the portion of the $(C_6H_6O)^{\bullet+}$ potential energy surface starting from $\mathbf{1}^{\bullet+}$ are constructed and schematically illustrated in Figure 5. Optimized geometries of the structures involved are listed in the Supporting Information. Selected geometrical parameters of some interesting structures are given in Figures 6 (equilibrium structures) and 7 (transition structures). As for a convention, $\mathbf{X}^{\bullet+}/\mathbf{Y}^{\bullet+}$ denotes a transition structure (TS) linking two equilibrium structures $\mathbf{X}^{\bullet+}$ and $\mathbf{Y}^{\bullet+}$. To increase the readability of the results shown in Figure 5, Scheme 3 structurally illustrates the various reaction pathways starting from $\mathbf{1}^{\bullet+}$.

Overall, the numerous reaction pathways found on the lower-lying portion of the potential energy surface (Figure 5 and Scheme 3) invariably lead to an elimination of CO giving $(C_5H_6)^{\bullet+}$ ion fragments (*m*/*z* 66). The energy surface can be divided into two distinct parts: although the first part involves the three cyclohexanone ion isomers $\mathbf{2}^{\bullet+}$, $\mathbf{5}^{\bullet+}$, and $\mathbf{4}^{\bullet+}$, the second consists of the conversion of the cyclic keto ions into either the various open-chain distonic forms $\mathbf{11}^{\bullet+}$ (or its conformers $\mathbf{12}^{\bullet+}$ and $\mathbf{13}^{\bullet+}$), $\mathbf{14}^{\bullet+}$, and $\mathbf{16}^{\bullet+}$ or the five-membered cyclic derivatives $\mathbf{6}^{\bullet+}$, $\mathbf{7}^{\bullet+}$, and $\mathbf{18}^{\bullet+}$. There are also some weak hydrogen bond complexes between CO and the CH bond of ionized cyclopentadienes such as $\mathbf{9}^{\bullet+}$ and $\mathbf{19}^{\bullet+}$.

The first step thus corresponds to a 1,3-hydrogen shift via the transition structure (TS) $\mathbf{1}^{\bullet+}/\mathbf{2}^{\bullet+}$ whose selected geometrical parameters are given in Figure 7. For the purpose of comparison, geometrical parameters of the TS **1/2** for the corresponding neutral process are also included. The 1,3-H shift is associated with a rather high energy barrier of 276 kJ/mol relative to the phenol radical cation $\mathbf{1}^{\bullet+}$. The corresponding neutral energy barrier amounts to 278 kJ/mol (cf. optimized geometry recorded

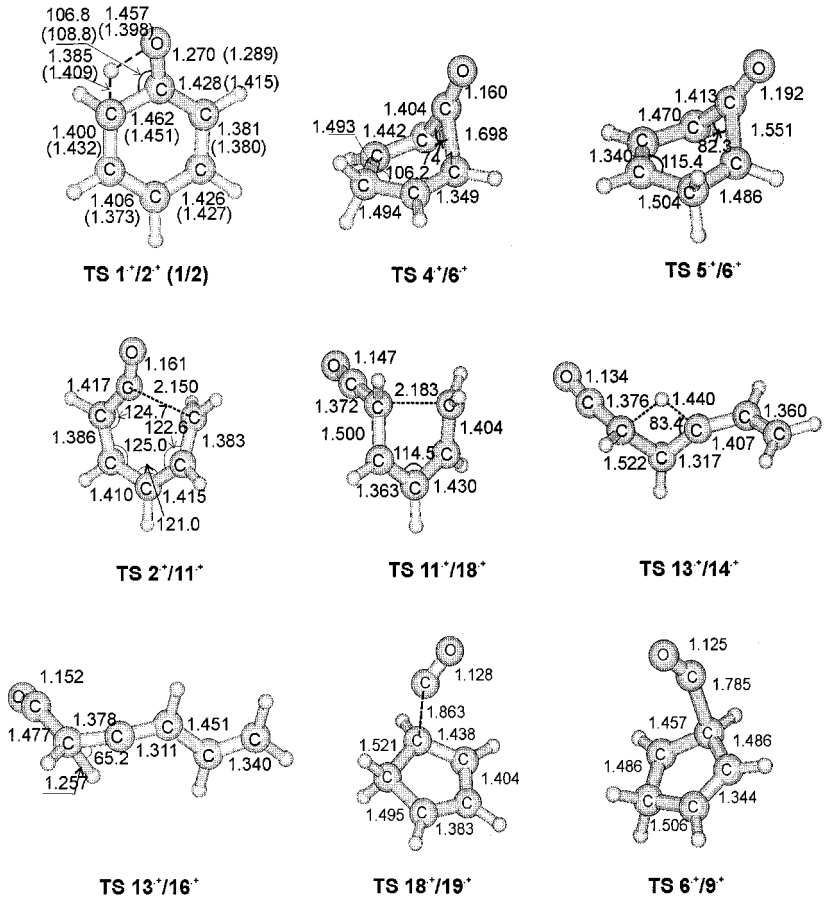

Figure 7. Selected geometric parameters of some important transition structures shown on the potential energy surface. For the TS for 1,3-H shift $\mathbf{1}^{\bullet+}/\mathbf{2}^{\bullet+}$, values given in parentheses correspond to the process of neutral phenol. Bond distances are given in angstroms and bond angles in degrees.

in Figure 7). Thus, there is practically no reduction in the barrier height following ionization. It appears that, once formed, the keto ion $\mathbf{2}^{\bullet+}$ easily undergoes a ring opening via TS $\mathbf{2}^{\bullet+}/\mathbf{11}^{\bullet+}$, yielding the open-chain distonic ketene radical cation $\mathbf{11}^{\bullet+}$. The successive 1,2-H shifts within the ring are also possible to give $\mathbf{5}^{\bullet+}$ and finally the most stable keto form $\mathbf{4}^{\bullet+}$. From here, the six-membered cyclic framework could be converted into the five-membered ring $\mathbf{6}^{\bullet+}$ lying 189 kJ/mol above $\mathbf{1}^{\bullet+}$ by direct one-step rearrangements via the TSs $\mathbf{4}^{\bullet+}/\mathbf{6}^{\bullet+}$ and $\mathbf{5}^{\bullet+}/\mathbf{6}^{\bullet+}$. From $\mathbf{6}^{\bullet+}$, an almost spontaneous CO loss with an energy barrier of only 18 kJ/mol could thus occur, giving the complex $\mathbf{9}^{\bullet+}$, which dissociates to the fragment products CO + cyclopentadiene ion $\mathbf{10}^{\bullet+}$, 116 kJ/mol less stable than phenol ion $\mathbf{1}^{\bullet+}$.

Although the ketene ring $\mathbf{7}^{\bullet+}$ is found to be only 53 kJ/mol above $\mathbf{1}^{\bullet+}$ and by far more stable than acetyl ion $\mathbf{6}^{\bullet+}$, it turns out that the CO loss from an indirect process giving finally the five-membered ion $\mathbf{8}^{\bullet+}$, namely, $\mathbf{6}^{\bullet+}-\mathbf{7}^{\bullet+}-(\mathbf{CO} + \mathbf{8}^{\bullet+})$ is a substantially more difficult route to follow. The cyclic isomer $\mathbf{6}^{\bullet+}$ is a possible intermediate in the CO-eliminative process of phenol cation $\mathbf{1}^{\bullet+}$ (Figure 5). Nevertheless, the high energy content of both TSs $\mathbf{4}^{\bullet+}/\mathbf{6}^{\bullet+}$ and $\mathbf{5}^{\bullet+}/\mathbf{6}^{\bullet+}$, which are lying 293 and 300 kJ/mol, respectively, above $\mathbf{1}^{\bullet+}$ but actually 20 kJ/mol above the TS $\mathbf{1}^{\bullet+}/\mathbf{2}^{\bullet+}$ for the initial 1,3-H shift, makes the rearrangement through $\mathbf{6}^{\bullet+}$ less competitive than other routes, even though this is more favored than an H-atom elimination characterized by a dissociation energy of 374 kJ/mol for a direct O−H bond cleavage (Figure 5). Selected geometrical parameters of the TSs mentioned are displayed in Figure 7.

The alternative route comprises the open-chain ketene ion $\mathbf{11}^{\bullet+}$ and its conformers $\mathbf{12}^{\bullet+}$ and $\mathbf{13}^{\bullet+}$ formed by ring opening of the ketone ion $\mathbf{2}^{\bullet+}$. From here, the supersystem could either rearrange to the open-chain acetyl cations $\mathbf{14}^{\bullet+}$ and $\mathbf{16}^{\bullet+}$ or undergo a cyclization forming back the five-membered ring $\mathbf{18}^{\bullet+}$ which is significantly more stable than $\mathbf{14}^{\bullet+}$ and $\mathbf{16}^{\bullet+}$ (137, 240, and 306 kJ/mol above $\mathbf{1}^{\bullet+}$, respectively). Figure 5 points out that the CO loss via $\mathbf{18}^{\bullet+}$ is beyond any doubt the lowest energy route.

Figure 8 illustrates the lowest energy rearrangement path for the CO-loss process of ionized phenol. As the B3LYP density functional method is essentially a single-reference approach, it is not appropriate for treating structures having more than one dominant electronic configuration. To verify this important feature, we carry out the single-point multiconfigurational CASSCF computations using the seven-electron−eight-orbital active spaces and the 6-31G(d,p) basis set[44] along with the B3LYP optimized geometries. The obtained CASSCF(7,8) wave functions clearly demonstrate that the ground electronic states of all stationary points considered in Figure 8 are dominated by the Hartree−Fock references. In all structures examined, the weights of the HF configurations are equal to, or larger than, 0.90 (the corresponding coefficients $C_0 \geq 0.95$).

Because the CASSCF method provides only nondynamical correlation energy and their relative energies are not size-consistent, it is usually not better than the B3LYP method in determining the relative energies of single-reference species. We also perform the subsequent CASPT2 computations based on CASSCF(7,8) wave functions; they are however also troublesome concerning the evaluation of the fragments energies. The calculated total and relative CASSCF and CASPT2 energies along with the weights of HF references are listed in the table and included in the Supporting Information. The CASPT2/6-31G(d,p) + ZPE values for the minima and TSs are also given

SCHEME 3

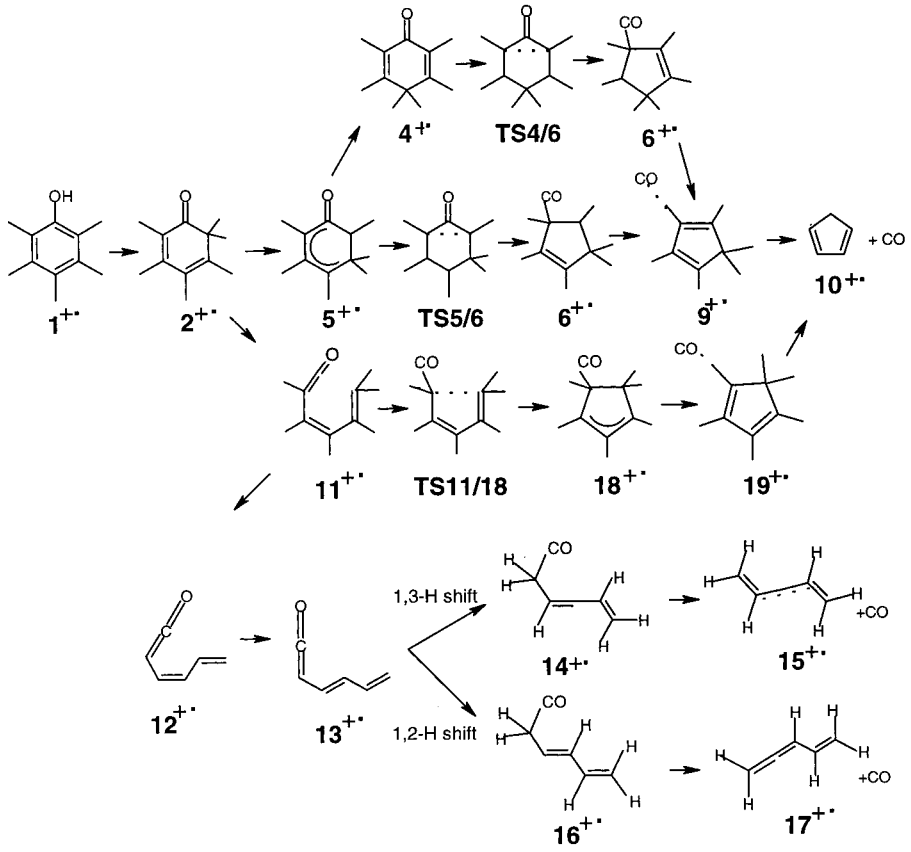

in Figure 8. Overall, the B3LYP relative energies are rather close to the CASPT2 counterparts despite a difference in the quality of the basis sets used. The differences amount to, at most, 20 kJ/mol, but the shape of the energy surface remains unchanged. Because of the clear-cut single-reference character of all important stationary points considered in the present case (Figure 8) and the rather limited size of the active spaces in the CASSCF wave functions, we would prefer to use the B3LYP relative energies for the discussion of the reaction paths and mechanism.

Results summarized in Figure 8 and structurally illustrated in Scheme 3 show that the reaction path involves, in a first step, the enol−keto conversion $\mathbf{1}^{\bullet+}-\mathbf{2}^{\bullet+}$. Starting from $\mathbf{2}^{\bullet+}$, a ring opening leads to structure $\mathbf{11}^{\bullet+}$ which, in turn, by ring closure produces ion $\mathbf{18}^{\bullet+}$. A direct and concerted isomerization $\mathbf{2}^{\bullet+}-\mathbf{18}^{\bullet+}$ has also been explored, but all our attempts are unsuccessful and invariably lead to the open form $\mathbf{11}^{\bullet+}$. This is at odds with the finding of Caballol et al.[17] who were able to locate a transition structure using the MINDO/3 method. The CO loss from $\mathbf{18}^{\bullet+}$ involve the slightly stabilized ion/neutral intermediate $\mathbf{19}^{\bullet+}$. The rate determining step of the overall process $\mathbf{1}^{\bullet+}-\mathbf{2}^{\bullet+}-\mathbf{11}^{\bullet+}-\mathbf{18}^{\bullet+}-\mathbf{19}^{\bullet+}-(\mathbf{CO} + \mathbf{C_5H_6}^{\bullet+})$ is the 1,3-H shift $\mathbf{1}^{\bullet+}/\mathbf{2}^{\bullet+}$. These results are in good agreement with experimental mass spectrometric studies[18] that demonstrated that the CO loss (*m*/*z* 66) corresponds to the least energy demanding fragmentation. Furthermore, it has been found earlier that the kinetic energy released during the CO loss from the keto ion $\mathbf{2}^{\bullet+}$ is less than that involved during the dissociation of the phenol ion $\mathbf{1}^{\bullet+}$ itself.[18] This is clearly in keeping with the potential energy profile presented in Figure 8. The appearance energy of the $[M-CO]^{\bullet+}$ ions has been determined by time-resolved electron impact[19] and photoionization[20] experiments and by photoelectron photoion coincidence.[21] From a comparison of the data, and after considering the kinetic shift, an energy threshold of 11.4 ± 0.1 eV at 298 K is deduced. Taking an adiabatic ionization energy of 8.49 ± 0.02 eV[43] and a correction for the 298 K enthalpy of ∼0.1 eV for phenol into account, the energy barrier separating $\mathbf{1}^{\bullet+}$ from its fragments is thus ca. 3.0 ± 0.15 eV, i.e., 290 ± 15 kJ/mol. This value is in excellent agreement with the calculated 0 K energy barrier $\mathbf{1}^{\bullet+}-\mathbf{2}^{\bullet+}$ of 276−290 kJ/mol (Figure 8).

It may finally be noted that the energy amount involved in the CO loss process is by far smaller than that needed for a deprotonation of phenol cation as mentioned above, namely, 857 kJ/mol. This suggests that the ease with which a deprotonation of phenol radical cations occurs in different solutions[7,11,12] is likely to arise from either a specific participation of the solvent molecules in the supermolecule or a strong continuum effect.

3. Mass Spectrometric Experiments

Having established the dominant existence of the phenol ion isomer by theoretical computations, we now wish to verify this again by means of state-of-the-art mass spectrometric experiments. These experiments are also attempted in search of the possible production of $C_6H_6O^{\bullet+}$ isomers such as dehydrophenyloxonium ions or cyclohexadienone ions.

These experiments are performed on a large scale (Micromass AutoSpec 6F, Manchester) tandem mass spectrometer of $E_1B_1E_2$-$qcE_3B_2cE_4$ geometry (E stands for electric sector, B for magnetic sector, q for a radio frequency-only quadrupole collision cell, and c for the "conventional" collision cells used in the present work).[40,41] Typical conditions are 8 kV accelerating voltage, 1 mA emission current (in the chemical ionization mode), 200 μA (in the electron ionization mode), and 70 eV ionizing electron energy.[40,41] Three different MS experiments are thus performed.

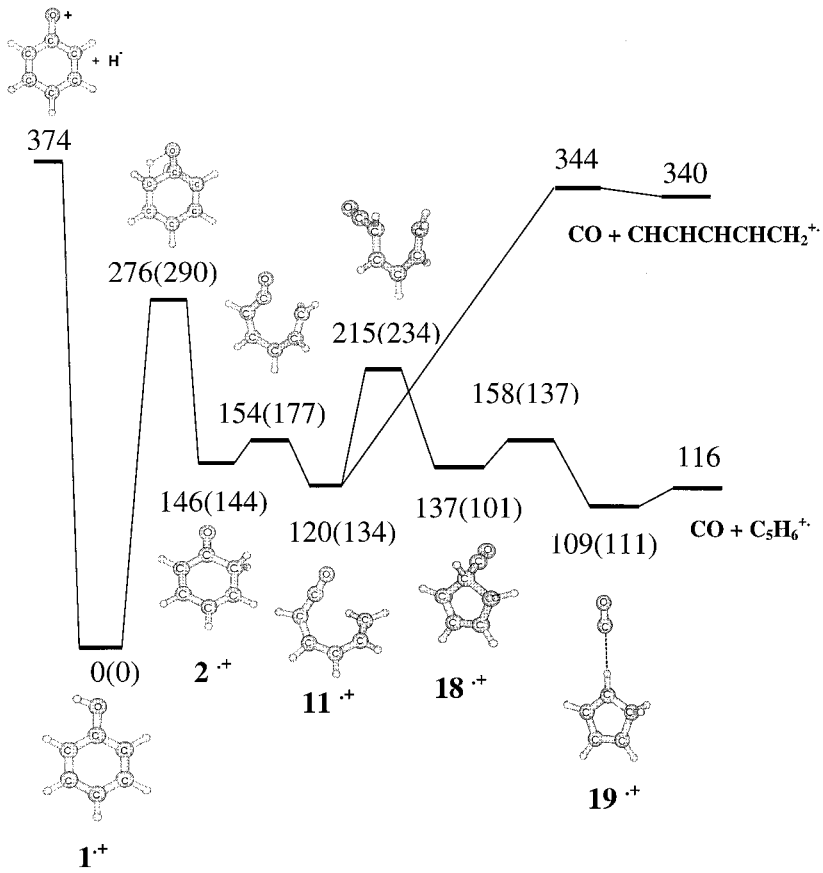

Figure 8. Schematic representation of the $(C_6H_6O)^{\bullet+}$ potential energy surface showing the lowest energy path for CO loss of phenol radical cation. Relative energies given in kJ/mol are obtained from B3LYP/6-311++G(d,p)+ZPE calculations. In parentheses are the relative energies obtained from CASPT2(7,8)/6-31G(d,p) + ZPE computations.

First, 4-bromophenol and 4-bromoanisole molecules are protonated in the chemical ionization ion source by using methane as the reagent gas, at an estimated pressure of 0.5−1.0 Torr. It is expected that collisional debromination of protonated 4-bromophenol could be an interesting source of a distonic isomer of ionized phenol if protonation takes place on oxygen. Alternatively, phenol ions should be produced in the case of ring protonation. The same behavior is expected for protonated 4-bromoanisole.

The high energy CA spectra of the $C_6H_6O^{\bullet+}$ ions (*m*/*z* 94) or $C_7H_8O^{\bullet+}$ ions (*m*/*z* 108) are obtained in the following way: mass-selected (with $E_1B_1E_2$) ions are decelerated from the initial 8 keV to ca. 20−30 eV and focalized into the rf-only quadrupole collision cell pressurized with argon (10^{-3} Torr estimated pressure). The collision induced dissociation products are thereafter reaccelerated at 8 keV and mass separated by scanning of the field of the second magnet B_2. Finally, the CA spectra of the $[MH-Br]^{\bullet+}$ ions are obtained by colliding the mass-selected ions with nitrogen in the cell preceding E_4 and scanning the field of E_4. The resulting spectra depicted in Figure 9 are found to be identical to the corresponding spectra of ionized phenol or anisole, respectively.

This observation is in line with the known preferential protonation at the ring, not at the oxygen atom, of the phenol and anisole molecules.[44] Distonic dehydrooxonium ions **c** are therefore not generated in these chemical ionization experiments, in line with the fact that they are more than 200 kJ/mol less stable than ions **b** (Scheme 4). A major fragmentation of ions **c** should be a loss of HOH or ROH with the production of benzyne ions (*m*/*z* 76), but the relative intensity of this peak is not increased, confirming that ions **c** are not produced to a significant extent in the protonation−debromination sequence.

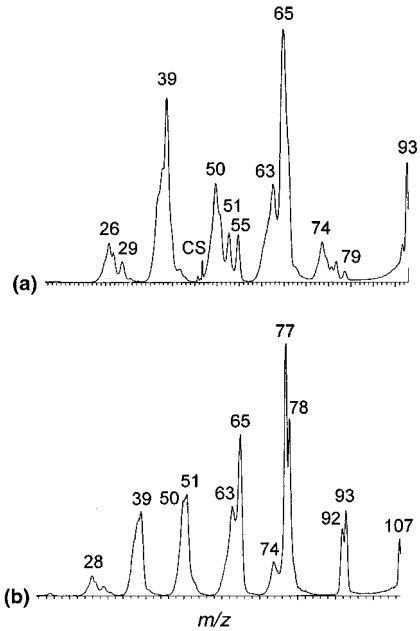

Figure 9. CA spectra of (a) $[MH-Br]^{\bullet+}$ radical cations (nitrogen collision gas) generated by low energy collisional activation (argon collision gas) of mass-selected protonated 4-bromophenol $\mathbf{1H}^+$ and (b) protonated 4-bromoanisole $\mathbf{2H}^+$. CS refers to a charge stripping.

This behavior contrasts thus with the case of 4-iodoaniline, where protonation in a chemical ionization source occurred not only on the ring but also on the nitrogen atom.[29] Nitrogen protonation is indicated by ion−molecule reactions with di-

SCHEME 4

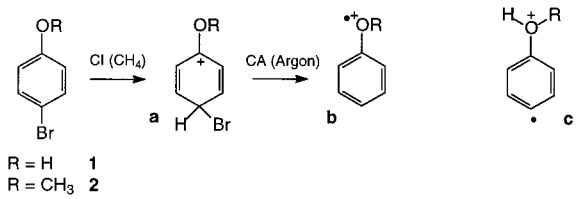

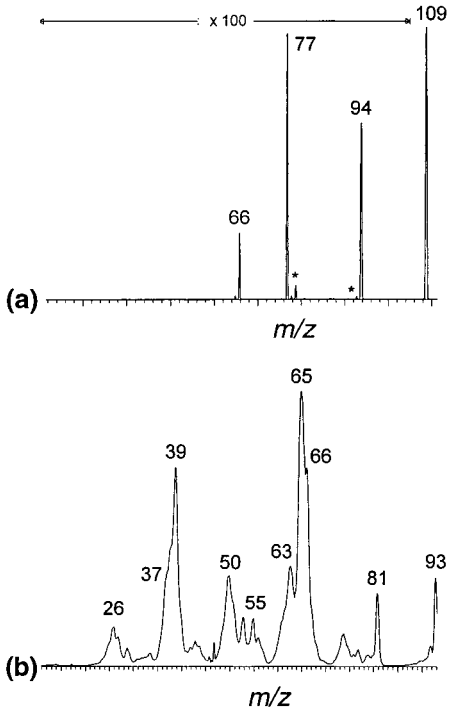

Figure 10. (a) MIKE spectrum of protonated anisole *m*/*z* 109, and (b) CA (nitrogen) spectrum of the *m*/*z* 94 ions.

methyl disulfide consecutive to collisional dehalogenation (FT-ICR experiments)[42] or by an increase of intensity of the peak at *m*/*z* 76 following high energy collisional activation.[29]

Interestingly, the regiospecificity of nitrogen protonation of aniline is found to be significantly increased in liquid secondary ion mass spectrometry (LSIMS) conditions.[29] Some preliminary experiments performed in LSIMS or electrospray (ES) ionization conditions on phenol or anisole are however found unsuccessful for the generation of protonated species.

Given the fact that a ring protonation is shown in the preceding experiment, unsubstituted anisole[44] is also protonated under methane chemical ionization conditions with an expectation that if the methyl group could thereafter be collisionally expelled within the quadrupole collision cell a cyclohexadienone structure (ortho $\mathbf{2}^{\bullet+}$ and/or para $\mathbf{4}^{\bullet+}$) could be produced. In agreement with theoretical calculations,[44] protonation occurs on the ring as indicated by the experiments described above on 4-bromoanisole, and a demethylation is indeed a prominent fragmentation of protonated anisole (Figure 10a). However, the CA spectrum of the reaccelerated *m*/*z* 94 ions (Figure 10b) is found to be identical to the CA spectrum of the phenol radical cation, not that of cyclohexadienone ions.

A similar observation is also made using another MS/MS/MS experiment where the demethylation step is realized in the high kinetic energy regime (collisional demethylation with oxygen in the cell preceding E_2 and fragmentation with nitrogen collision gas in the cell preceding E_4).

Using available heats of formation,[44] a demethylation of protonated anisole is less endothermic by about 146 kJ/mol if

SCHEME 5

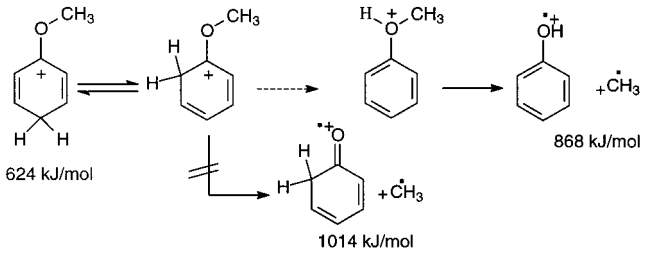

ionized phenol $\mathbf{1}^{\bullet+}$ is formed rather than ionized cyclohexadienone $\mathbf{2}^{\bullet+}$ (cf. Scheme 5). Results obtained from density functional theory computations using the (U)B3LYP/6-311++G(d,p) + ZPE level on the interconversion of protonated anisoles and summarized in Figure 11 point out that a demethylation of the latter invariably involves formation of its O-protonated form and ends up with the production of ionized phenol $\mathbf{1}^{\bullet+}$. The O protonation is about 57 kJ/mol less favored than the ring para C protonation.[44] The entire process is associated with an energy barrier of 232 kJ/mol relative to the most stable protonated form, a value comparable to that required for a direct C−O bond cleavage of O-protonated anisole.

In the last experiment, 2-hydroxybenzaldehyde (salicylaldehyde) is submitted to electron ionization. Because of an ortho effect, carbon monoxide is, inter alia, expelled from the metastable molecular ions (MIKE spectrum, the concerned field-free region being the quadrupole cell, Figure 12a). The CA spectrum of these so-produced *m*/*z* 94 ions is depicted in Figure 12c. This spectrum indicates that these ions are actually *not* phenol radical cations. Moreover, when the *m*/*z* 94 ions are collisionally generated in the quadrupole, the CA spectrum is very significantly modified (Figure 12d) with the appearance of an intense signal at *m*/*z* 76 corresponding to a loss of water.

It is tentatively proposed in Scheme 6 that, under high energy conditions, the decarbonylation is initiated by a hydrogen migration from the carbonyl to the hydroxyl moiety; a loss of CO thus affords the ortho-oxonium distonic isomer of phenol. As discussed previously, an ortho-distonic ion isomer should survive within a short time before rearranging into ionized phenol (cf. Scheme 2). For lower energy ions, the initial rearrangement should be different, but given the fact that telltale peaks are *not* detected in the CA spectrum, the actual identity of these meta-stable ions generated under such circumstances remains unclear.

SCHEME 6

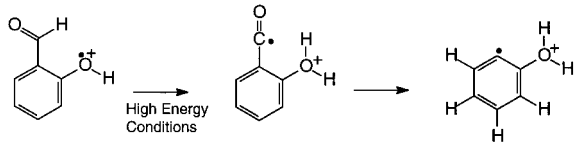

4. Concluding Remarks

Using a combination of tandem mass spectrometric methods, it is shown that a debromination of protonated 4-bromophenol and 4-bromoanisole essentially produces phenol and anisole radical cations, respectively; no less conventional molecular ions are detected. Similarly, collisional demethylation of protonated anisole gives rise to ionized phenol. Electron ionization of salicylaldehyde appears to produce an ortho-oxonium distonic isomer of the conventional phenol ion whereas another yet undefined species is produced from metastable molecular ions of salicylaldehyde.

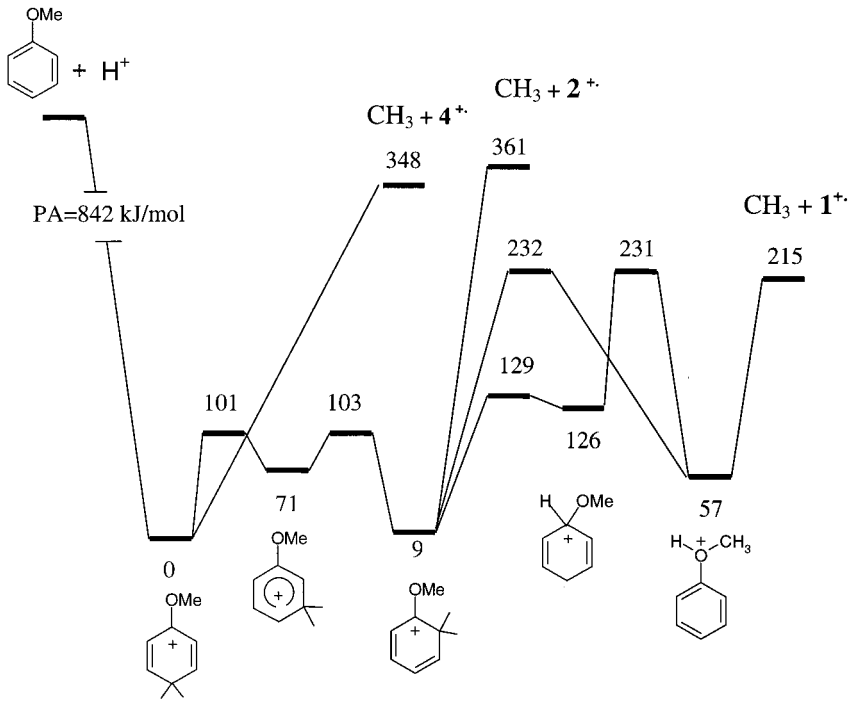

Figure 11. Schematic potential energy profile showing the rearrangement of protonated anisole. Relative energies given in kJ/mol are obtained from B3LYP/6-311++G(d,p) + ZPE computations.

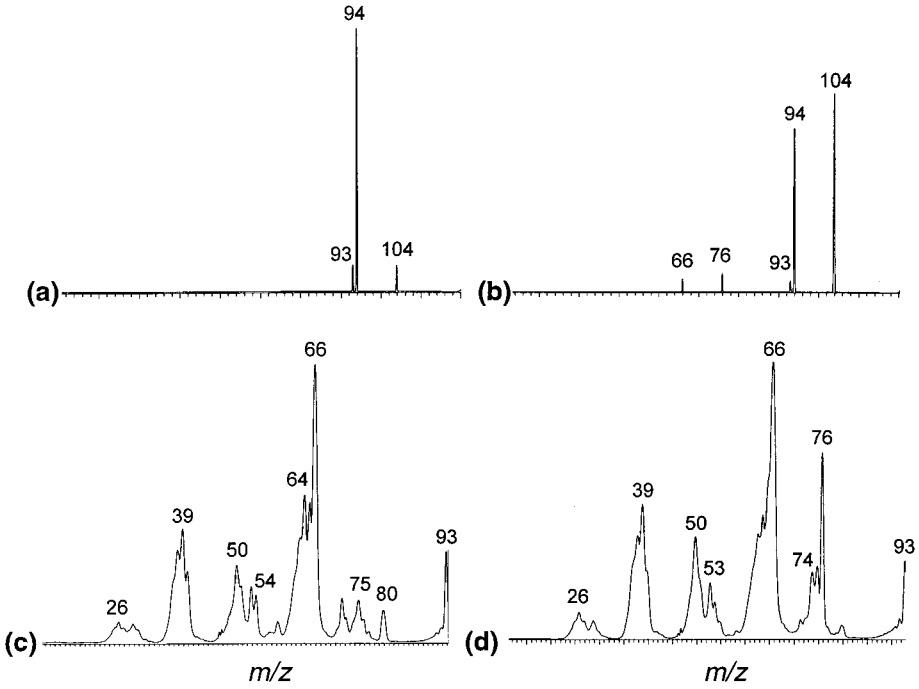

Figure 12. (a) MIKE and (b) CA spectra of the *m*/*z* 122 ions of ionized salicylaldehyde (peaks at *m*/*z* 121, ca. 5× more intense, not shown), and c and d CA (nitrogen) spectra of the *m*/*z* 94 ions produced in these conditions.

Quantum chemical results at the UB3LYP/6-311++G(d,p) + ZPE level suggest the predominant stability of the phenol radical cation, which lies at least 130 kJ/mol below the other six-membered isomers. The preponderant fragmentation is confirmed to be a CO loss involving the intermediacy of the keto six-membered ring, open-chain ketene, and five-membered cyclopentadiene ion isomers. The rate determining step corresponds to the enol−ketone interconversion of the phenol ion with a barrier height of 276−290 kJ/mol relative to phenol ion, which is markedly smaller than that required for a hydrogen atom loss or a deprotonation. This suggests an important role played by the solvent in the readiness of the deprotonation of phenol ions in nonpolar media.

Some useful thermochemical parameters are evaluated including the adiabatic ionization energy of phenol, $IE_a(\text{phenol}) = 8.35 \pm 0.2$ eV (exptl: 8.47 eV), and the proton affinities (at 298K) of the phenoxy radical, $PA(C_6H_5O) = 863 \pm 10$ kJ/mol (exptl: 860 kJ/mol), phenol, PA(phenol) = 826 ± 10 kJ/mol (exptl: 818 kJ/mol), and anisole, PA(anisole) = 848 ± 10 kJ/mol.

Acknowledgment. The Leuven group is indebted to the KU-Leuven Research Council (GOA-program) for financial support. The Mons laboratory thanks the "Fonds National de la Recherche Scientifique" for its contribution in the acquisition of a large scale tandem mass spectrometer, Micromass AutoSpec 6F, and a postdoctoral fellowship to P.G. M.T.N. and G.B. are also grateful to the CNRS and Ministerie van de Vlaamse Gemeenschap for supporting a bilateral cooperation research project.

Supporting Information Available: Table of CASSCF and CASPT2 energies and optimized geometries (Z matrixes and Cartesian coordinates) of all structures considered at the B3LYP/6-311++G(d,p) level, together with total and zero-point energies. This information is available free of charge via the Internet at http://pubs.acs.org.

References and Notes

(1) Rappoport, Z. The Chemistry of Phenols. In *The Chemistry of Functional Groups*; Wiley: New York, 2002, to be published.

(2) Halliwell, B.; Gutteridge, J. M. C. *Free Radical in Biology and Medicine*, 2nd edition; Clarendon Press: Oxford, U.K., 1989.

(3) Burton, G. W.; Ingold, K. U. *Acc. Chem. Res*. **1986,** *19*, 194.

(4) Beckman, K. B.; Ames, B. N. *Physiol. Rev*. **1998**, *78*, 547.

(5) Scott, G. *Atmospheric Oxidation and Antioxidants*, Elsevier: Amsterdam, 1993; Vols. I and II.

(6) Wright, J. S.; Johnson, E. R.; DiLabio, G. A. *J. Am. Chem. Soc*. **2001**, *123*, 1173 and references therein.

(7) Ganapathi, M. R.; Hermann, R.; Naumov, S.; Brede, O. *Phys. Chem. Chem. Phys.* **2000**, *2*, 4947.

(8) Bordwell, F. G.; Cheng, J. P. *J. Am. Chem. Soc*. **1991**, *113*, 1736.

(9) Brede, O.; Orthner, H.; Zubarev, V. E.; Hermann, R. *J. Phys. Chem.* **1996**, *100*, 7097.

(10) Mohan, H.; Hermann, R.; Maunov, S.; Mittal, J. P.; Brede, O. *J. Phys. Chem. A*. **1998**, *102*, 5754.

(11) Hermann, R.; Naumov, S.; Mahalaxmi, G. R.; Brede, O. *Chem. Phys. Lett*. **2000**, *324*, 265.

(12) Gadosy, T. A.; Shukla, D.; Johnston, L. J. *J. Phys. Chem. A*. **1999**, *103*, 8834.

(13) Anderson, S. C.; Goodman, L.; Krogh-Jespersen, K.; Ozkabak, A. G.; Zare, R. N *J. Chem. Phys*. **1985,** *82*, 5329.

(14) LeClaire, J. E.; Anand, R.; Johnson, P. M. *J. Chem. Phys*. **1997**, *106*, 6785.

(15) Ishiuchi, S. I.; Shitomi, H.; Takazawa, K.; Fujii, M. *Chem. Phys. Lett*. **1998**, *283*, 243.

(16) Borchers, F.; Levsen, K.; Theissling, C. B.; Nibbering, N. M. M. *Org. Mass Spectrom.* **1977**, *12*, 746.

(17) Caballol, R.; Poblet, J. M.; Sarasa, P. *J. Phys. Chem.* **1985**, *89*, 5836.

(18) Russel, D. H.; Gross, M. L.; Nibbering, N. M. M. *J. Am Chem. Soc*. **1978**, *100*, 6133. (b) Russel, D. H.; Gross, M. L.; Van der Greef, J.; Nibbering, N. M. M. *Org. Mass Spectrom*. **1979**, *14*, 474. (c) Maquestiau, A.; Van Haverbeke, Y.; Flammang, R.; De Meyer, C.; Das, K. G.; Reddy, G. S. *Org. Mass Spectrom*. **1977**, *12*, 631. (d) Maquestiau, A.; Flammang, R.; Glish, G. L.; Laramee, J. A.; Cooks, R. G. *Org. Mass Spectrom*. **1980**, *15*, 131. (e) Maquestiau, A.; Flammang, R.; Pauwels, P.; Vallet, P.; Meyrant, P. *Org. Mass Spectrom*. **1982**, *17*, 643. (f) Turecek, F.; Drinkwater, D. E.; Maquestiau, A.; McLafferty, F. W. *Org. Mass Spectrom*. **1989**, *24*, 669.

(19) Lifshitz, C.; Gefen, S. *Org. Mass Spectrom.* **1984**, *19*, 197.

(20) Lifshitz, C.; Malinovich, Y. *Int. J. Mass Spectrom. Ion Processes* **1984**, *60*, 99.

(21) Fraser-Monteiro, M. L.; Fraser-Monteiro, L.; de Wit, J.; Baer, T. *J. Phys. Chem*. **1984**, *88*, 3622.

(22) Camaioni, D. M. *J. Am. Chem. Soc*. **1990,** *112*, 9475.

(23) Hoke, S. H.; Yang, S. S.; Cooks, R. G.; Hrovat, D. A.; Borden, W. T. *J. Am. Chem. Soc*. **1994**, *116*, 4888.

(24) Y. Q.; Wheeler, R. A. *J. Phys. Chem*. **1996**, *100*, 10554.

(25) Grafton, A. K.; Wheeler, R. A. *J. Comput. Chem*. **1998**, *19*, 1663.

(26) Trindle, C. *J. Phys. Chem. A*. **2000**, *104*, 5298.

(27) Flammang, R.; Barbieux-Flammang, M.; Gualano, E.; Gerbaux, P.; Le, H. T.; Nguyen, M. T.; Turecek, F.; Vivekananda, S. *J. Phys. Chem. A* **2001**, *105*, 8579.

(28) Flammang, R.; Barbieux-Flammang, M.; Gerbaux, P.; Le, T. H.; Turecek, F.; Nguyen, M. T. *Int. J. Mass Spectrom.* Submitted, 2001.

(29) Le, T. H.; Flammang, R.; Barbieux-Flammang, M.; Gerbaux, P.; Nguyen, M. T. *Int. J. Mass Spectrom.* Submitted, 2001.

(30) Frisch, M. J.; Trucks, G. W.; Schlegel, H. B.; Gill, P. M. W.; Johnson, B. G.; Robb, M. A.; Cheeseman, J. R.; Keith, T.; Petersson, G. A.; Montgomery, J. A.; Raghavachari, K.; Al-Laham, M. A.; Zakrzewski, V. G.; Ortiz, J. V.; Foresman, J. B.; Cioslowski, J.; Stefanov, B. B.; Nanayakkara, A.; Challacombe, M.; Peng, C. Y.; Ayala, P. Y.; Chen, W.; Wong, M. W.; Andres, J. L.; Replogle, E. S.; Gomperts, R.; Martin, R. L.; Fox, D. J.; Binkley, J. S.; Defrees, D. J.; Baker, J.; Stewart, J. P.; Head-Gordon, M.; Gonzalez, C.; Pople, J. A. *Gaussian 94*, revision C.3; Gaussian, Inc.: Pittsburgh, PA, 1995.

(31) (a) Becke, A. D. *J. Chem. Phys*. **1993**, *98*, 1372. (b) Lee, C.; Yang, W.; Parr, R. G. *Phys. Rev. B*. **1988**, *37*, 785.

(32) Lavorato, D. J.; Terlouw, J. K.; McGibbon, G. A.; Dargel, T. K.; Koch, W.; Schwarz, H. *Int. J. Mass Spectrom*. **1998**, *179*, 7.

(33) Nguyen, M. T.; Nguyen, T. L.; Le, H. T. *J. Phys. Chem. A* **1999**, *103*, 5758.

(34) Le, H. T.; Nguyen, T. L.; Lahem, D.; Flammang, R.; Nguyen, M. T. *Phys. Chem. Chem. Phys*. **1999**, *1*, 755.

(35) Gomez, P. C.; Pacios, L. F. *J. Phys. Chem. A* **1999**, *103*, 739.

(36) Fuelscher, M. P.; Olsen, J.; Malmqvist, P. A.; Roos, B. O. *Molcas*, version 4.0; Department of Theoretical Chemistry, Lund University: Lund, Sweden, 1999.

(37) See, for example: Turecek, F.; Cramer, C. J. *J. Am. Chem. Soc*. **1995**, *117*, 12243.

(38) (a) Smith, B. J.; Nguyen, M. T.; Bouma, W. J.; Radom, L. *J. Am. Chem. Soc*. **1991**, *113*, 6452. (b) Bertrand, W.; Bouchoux, G. *Rapid Commun. Mass Spectrom*. **1998**, *12*, 1697.

(39) Nguyen, M. T.; Landuyt, L.; Vanquickenborne, L. G. *Chem. Phys. Lett*. **1991**, *182*, 225.

(40) Flammang, R.; Van Haverbeke, Y.; Braybrook, C.; Brown, J. *Rapid Commun. Mass Spectrom.* **1995**, 9, 795.

(41) Gerbaux, P.; Van Haverbeke, Y.; Flammang, R. *J. Mass Spectrom*. **1997**, *32*, 1170.

(42) Chyall, L. J.; Kenttämaa, H. I. *J. Am. Chem. Soc*. **1994**, *116*, 3135; *J. Mass Spectrom*. **1995,** *30*, 81.

(43) NIST webbook. http://webbook.nist.gov/chemistry

(44) Tishchenko, O.; Pham-Tran, N. N.; Kryachko, E. S.; Nguyen, M. T. *J. Phys. Chem. A* **2001**, *105*, 8709 and references therein.